Yeast Irc6p is a novel type of conserved clathrin coat accessory factor related to small G proteins

Sabine Gorynia[a,*], Todd C. Lorenz[a,†], Giancarlo Costaguta[a], Lydia Daboussi[a], Duilio Cascio[b,c], and Gregory S. Payne[a,b]

[a]Department of Biological Chemistry, School of Medicine, [b]Molecular Biology Institute, and [c]Department of Energy Institute of Genomics and Proteomics, University of California at Los Angeles, Los Angeles, CA 90095

ABSTRACT **Clathrin coat accessory proteins play key roles in transport mediated by clathrin-coated vesicles. Yeast Irc6p and the related mammalian p34 are putative clathrin accessory proteins that interact with clathrin adaptor complexes. We present evidence that Irc6p functions in clathrin-mediated traffic between the *trans*-Golgi network and endosomes, linking clathrin adaptor complex AP-1 and the Rab GTPase Ypt31p. The crystal structure of the Irc6p N-terminal domain revealed a G-protein fold most related to small G proteins of the Rab and Arf families. However, Irc6p lacks G-protein signature motifs and high-affinity GTP binding. Also, mutant Irc6p lacking candidate GTP-binding residues retained function. Mammalian p34 rescued growth defects in *irc6*Δ cells, indicating functional conservation, and modeling predicted a similar N-terminal fold in p34. Irc6p and p34 also contain functionally conserved C-terminal regions. Irc6p/p34-related proteins with the same two-part architecture are encoded in genomes of species as diverse as plants and humans. Together these results define Irc6p/p34 as a novel type of conserved clathrin accessory protein and founding members of a new G protein–like family.**

Monitoring Editor
Benjamin S. Glick
University of Chicago

Received: Jul 9, 2012
Revised: Aug 22, 2012
Accepted: Sep 13, 2012

INTRODUCTION

Clathrin-coated vesicles (CCV) serve as evolutionarily conserved carriers for selective transport of proteins from the plasma membrane to endosomes and between the *trans*-Golgi network (TGN) and endosomes. Assembly of a clathrin coat orchestrates CCV formation by driving membrane invagination and scission, while concomitantly selecting appropriate cargo proteins.

Clathrin, a hexamer of heavy and light chains, forms an outer polyhedral scaffold in the coat that interacts with other coat proteins but does not directly bind to membranes. Instead, clathrin associates with adaptors that help anchor the coat to the membrane through interactions with lipids and/or the cytoplasmic domains of cargo proteins (Traub, 2005; Edeling *et al.*, 2006; McMahon and Boucrot, 2011). Adaptors also function as a binding platform for recruitment of other coat-interacting proteins, termed accessory factors, that play key roles in different stages of CCV formation, including coat assembly, membrane deformation and scission, and uncoating (Traub, 2005; Edeling *et al.*, 2006; McMahon and Boucrot, 2011). Because adaptors coordinate coat formation, membrane vesiculation, and cargo collection, they are central to CCV formation.

Two related heterotetrameric adaptor complexes, AP-1 and AP-2, are major components of CCV (Robinson, 2004; Edeling *et al.*, 2006). AP-1 is associated with the TGN and endosomes, whereas AP-2 is associated with the plasma membrane. Each is composed of two large subunits (γ and β_1 in AP-1, α and β_2 in AP-2), a medium subunit (μ_1 and μ_2), and a small subunit (σ_1 and σ_2). The subunits are arranged as a core consisting of the large-subunit N-terminal regions together with the μ and σ subunits. The large-subunit C-terminal regions extend from the core as flexible

This article was published online ahead of print in MBoC in Press (http://www.molbiolcell.org/cgi/doi/10.1091/mbc.E12-07-0507) on September 19, 2012.

Present addresses: *ONCOTEST GMBH, Am Flughafen 12-14, 79108 Freiburg, Germany; †Department of Biology, University of La Verne, Los Angeles, CA 91750.

Address correspondence to: Gregory S. Payne (gpayne@mednet.ucla.edu).

Abbreviations used: CCFW, calcofluor white; CCV, clathrin-coated vesicle; CDD, Conserved Domain Database; DTT, dithiothreitol; GFP, green fluorescent protein; GST, glutathione *S*-transferase; IPTG, isopropyl β-D-1-thiogalactopyranoside; LB, Luria–Bertani broth; NTPase, nucleoside triphosphate hydrolase; PDB, Protein Data Bank; PEG, polyethylene glycol; PMSF, phenylmethylsulfonyl fluoride; TGN, *trans*-Golgi network; WCL, whole-cell lysates.

linker regions connected to appendage domains. The AP core interacts with the membrane and cargo, while the hinge/appendage regions provide binding sites for clathrin and nearly all accessory proteins. A large number of accessory proteins have been described that bind either directly or indirectly to the AP-2 appendages, providing insights into endocytic vesicle formation at the plasma membrane (Edeling *et al.*, 2006; McMahon and Boucrot, 2011). In contrast, fewer AP-1–interacting proteins have been characterized, leaving the mechanism of TGN/endosome CCV formation less well defined (Traub, 2005).

The yeast protein Irc6p/Yfr043cp and its mammalian homologue p34 are putative clathrin coat accessory factors based on their identification as AP-1γ– and AP-2α–interacting proteins in yeast two-hybrid screens (Page *et al.*, 1999; Ito *et al.*, 2001; Yu *et al.*, 2008). Analysis of p34 revealed an unusual adaptor-binding mode involving association with the N-terminal core regions of the γ and α subunits (Page *et al.*, 1999). To investigate a possible role for these proteins in clathrin-mediated transport, we characterized the structure and function of Irc6p and tested for functional complementation by p34 in yeast. Our results indicate that Irc6p is related to G proteins, participates in clathrin-mediated TGN-endosome traffic, and can link AP-1 to the Rab Ypt31p. Mammalian p34 functionally substitutes for Irc6p in yeast. Together our findings provide evidence that Irc6p and p34 represent a novel type of evolutionarily conserved clathrin coat accessory factor.

RESULTS

Irc6p functions in clathrin-mediated TGN/endosome traffic

To test for Irc6p function in clathrin-mediated traffic, we applied an assay for genetic interaction with a temperature-sensitive allele of the clathrin heavy chain gene (*chc1-521*, referred to hereafter as *chc1-ts*; Seeger and Payne, 1992). Commonly, deletions of genes whose products act in clathrin-dependent transport pathways exacerbate *chc1-ts* growth defects, whereas the same deletions in *CHC1* cells are innocuous, likely due to redundant proteins and/or alternative pathways (Yeung *et al.*, 1999; Bensen *et al.*, 2000, 2001; Costaguta *et al.*, 2001; Fernandez and Payne, 2006). Accordingly, we compared the growth of *chc1-ts irc6*Δ double mutants with wild-type and single mutants (Figure 1A). All strains displayed similar growth rates at 24°C, and *irc6*Δ cells grew like wild-type cells at the semipermissive temperature of 30°C. However, *chc1-ts irc6*Δ cell growth at 30°C was more severely retarded than that of *chc1-ts* cells. Introduction of a low-copy plasmid expressing FLAG-tagged Irc6p into double mutant cells restored growth to the level of *chc1-ts* cells (Figure 1A).

CCVs mediate endocytosis and transport between the TGN and endosomes. Endocytosis was assayed by determining the sensitivity of cells to K28 killer toxin, which depends on AP-2–mediated endocytosis for intoxication of cells (Carroll *et al.*, 2009). In this assay, cells being tested for K28 sensitivity are spread as a lawn on an agar plate, and concentrated K28-secreting cells are spotted onto the lawn. K28 sensitivity results in a zone of cell death surrounding the K28-producing cells (Figure 1B). Based on a screen of the yeast gene deletion collection, deletion of *IRC6* was reported to confer K28 resistance (Carroll *et al.*, 2009). However, in our strain background, *irc6*Δ did not alter sensitivity to the toxin (Figure 1B). We did observe increased resistance to K28 in the *MAT*α *irc6*Δ strain from the deletion collection but not in the corresponding *MAT***a** *irc6*Δ strain (Figure S1). Furthermore, no effects on K28 sensitivity were detected when *IRC6* was deleted in the parental strain for the *MAT*α deletion collection or a completely different K28 hypersensitive strain (Figure S1). Thus our results suggest that Irc6p does not provide important function in AP-2–mediated endocytosis.

Transport between the TGN and endosomes was assessed by monitoring proteolytic maturation of the secreted pheromone α-factor. This assay provides a sensitive measure of clathrin-mediated trafficking of the maturation protease Kex2p between the TGN and endosomes (Payne and Schekman, 1989). Inhibition of clathrin function results in Kex2p mislocalization to the cell surface, which in turn causes incomplete maturation of the α-factor precursor (Payne and Schekman, 1989). Unlike clathrin mutations, inactivation of TGN/endosome clathrin adaptors, such as AP-1, often do not affect pheromone maturation. However, such mutations enhance maturation defects of *chc1-ts* cells (Phan *et al.*, 1994; Rad *et al.*, 1995; Yeung *et al.*, 1999; Costaguta *et al.*, 2001). At both 24°C and 30°C, *irc6*Δ and wild-type cells secreted only mature α-factor (Figure 1C, lanes 1, 3, 5, and 7). However, at 24°C, at which *chc1-ts* cells are not affected, combination of *irc6*Δ and *chc1-ts* resulted in secretion of precursor forms (Figure 1C, lanes 2 and 4). The double mutant also exhibited an enhanced maturation defect compared with *chc1-ts* cells at 30°C (Figure 1C, lanes 6 and 8).

Growth of cells in the presence of the chitin-binding dye calcofluor white (CCFW) provides an assay for AP-1–dependent traffic. In *chs6*Δ cells, the chitin synthase Chs3p is retained intracellularly by clathrin-dependent and AP-1–dependent cycling between the TGN and endosomes, thereby reducing cell surface chitin rings and conferring CCFW resistance. In *chs6*Δ cells, inactivation of AP-1 perturbs the intracellular cycling pathway and allows Chs3p to escape to the cell surface, restoring chitin rings and sensitivity to CCFW (Valdivia *et al.*, 2002). Deletion of *IRC6* in *chs6*Δ cells increased sensitivity to CCFW, although not to the same extent as inactivating AP-1 by deleting the β1 subunit, and restored chitin rings (Figure 1, D–F). Expression of FLAG-Irc6p in *irc6*Δ *chs6*Δ cells conferred CCFW resistance and eliminated chitin rings. There was no further increase in CCFW sensitivity when *irc6*Δ was introduced into *β1*Δ *chs6*Δ cells (Figure 1E), consistent with Irc6p function in AP-1–mediated Chs3p transport. The *irc6*Δ phenotypes provide evidence that Irc6p functions in AP-1/clathrin–mediated traffic between the TGN and endosomes. We were unable to detect Irc6p expressed at endogenous levels by immunofluorescence or using green fluorescent protein (GFP) fusions, most likely because of low expression levels. At elevated expression levels, Irc6p appeared cytoplasmic (unpublished data).

Irc6p contains a novel small G protein–like domain

Irc6p displayed no clear sequence similarity to proteins of known function in database searches. To gain insights into the molecular architecture of Irc6p, we determined the structure by x-ray crystallography. Although full-length Irc6p did not crystallize, we obtained crystals of a large, C-terminally truncated fragment (aa 1–213). Phases were determined by the selenomethionine single-wavelength anomalous dispersion method, and the final structure was refined against 1.8 Å resolution data to a crystallographic R_{work}/R_{free} = 19.7%/21.8% (Table 1 and Figures 2A and S2A). The structure revealed that amino acids 1–176 were arranged as a Rossmann fold, a structural motif involved in nucleotide binding (Rao and Rossmann, 1973). A core, six-stranded β-sheet is flanked by six α-helices (Figure 2, A and B). No electron density was detected for the C-terminal 28 residues in the fragment (aa 186-213), suggesting that this region may be flexible or absent due to proteolysis.

The Protein Data Bank (PDB) was searched with the Irc6p aa 1–176 structure using the Dali server (Holm and Rosenstrom, 2010). All significant hits were G proteins, including more than 80 with

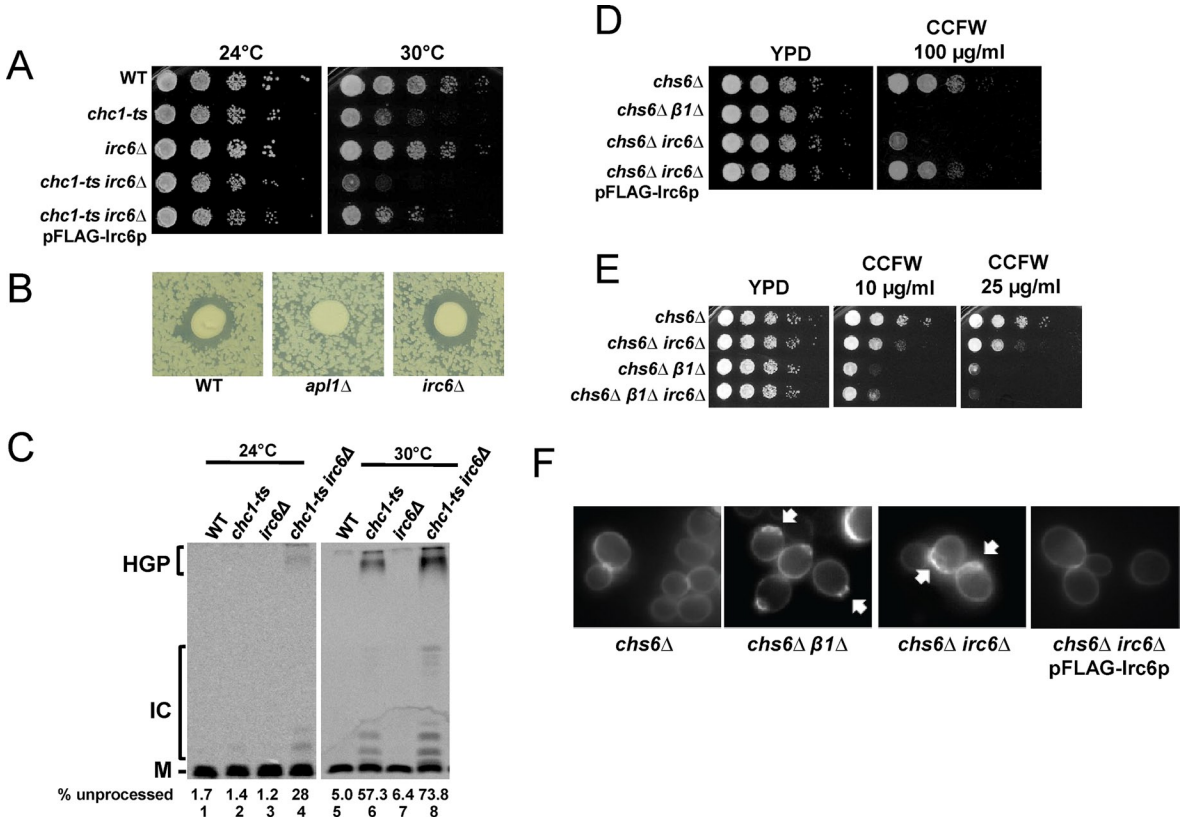

FIGURE 1: Irc6p function is associated with clathrin-mediated transport between the TGN and endosomes. (A) Genetic interactions between *irc6*Δ and *chc1-ts*. Wild-type (WT, SEY6210), *chc1-ts* (GPY1064), *irc6*Δ (GPY4986), *chc1-ts irc6*Δ (GPY3986), and *chc1-ts irc6*Δ pFLAG-Irc6p (GPY5008) strains were grown overnight at 24°C in YPD media, serially diluted, spotted onto YPD plates, and incubated for 2 d at the indicated temperatures. (B) No effect of *irc6*Δ on K28 toxin sensitivity. Indicated strains (WT, wild-type; *apl1*Δ, GPY1783-21D; *irc6*Δ, GPY4136) were grown overnight in YPD and then plated as a lawn on low-pH agar plates. Concentrated K28 toxin-secreting cells (MS300) were then spotted on the lawn, and the plates were incubated at 24°C for 2 d. The zone of clearing around the central spot of toxin-producing cells is an indicator of toxin sensitivity. (C) The α-factor maturation defect in *chc1-ts* cells is enhanced by *irc6*Δ. Wild-type and mutant strains as described in (A) were metabolically labeled at 24°C for 45 min or 30°C for 30 min. Secreted α-factor was immunoprecipitated from the media and analyzed by SDS–PAGE and autoradiography. HGP, highly glycosylated precursor; IC, intermediate cleavage products; M, mature. The amount of each form was quantified, and processing efficiency was expressed as the percentage of total present in HGP and IC forms. (D) *irc6*Δ increases CCFW sensitivity in *chs6*Δ cells. *chs6*Δ (GPY3102), *chs6*Δ *apl2*Δ (*chs6*Δ *β1*Δ; GPY3103), *chs6*Δ *irc6*Δ (GPY4042), and *chs6*Δ *irc6*Δ pFLAG-Irc6p (GPY5009) strains were grown overnight at 30°C, serially diluted, spotted onto YPD plates without (YPD) or with 100 µg/ml calcofluor white (CCFW), and incubated for 2 d at 30°C. (E) *irc6*Δ does not enhance CCFW sensitivity in *apl2*Δ *chs6*Δ cells. Cells carrying *chs6*Δ, *chs6*Δ *apl2*Δ, or *chs6*Δ *irc6*Δ as in (D) and *chs6*Δ *apl2*Δ *irc6*Δ (GPY4603) were assayed for sensitivity to the indicated CCFW concentrations as in (D). (F) Increased cell surface chitin in *irc6*Δ *chs6*Δ cells. Strains as in (D) were stained with CCFW and imaged by epifluorescence microscopy. Arrows point to bud scars.

Z-scores higher than 10. PDB structures with the strongest similarity were Arf-like GTPase 1 (Arl1, PDB ID: 1upt) and the GTPase Rab5 (PDB ID: 2efh; Figure 2B), which act in membrane trafficking (Panic *et al.*, 2003; Stenmark, 2009; Donaldson and Jackson, 2011). Irc6p aa 1–176 and Rab5 can be superimposed with a root mean-square deviation of 2.6 Å over 131 aligned Cα residues (Figure 2C).

G proteins share a common 20-kDa catalytic domain (G domain), with consensus motifs responsible for GTP binding and hydrolysis (Bourne *et al.*, 1991; Wittinghofer and Vetter, 2011). Irc6p lacks these motifs, suggesting that it does not bind GTP with high affinity. The crystals of Irc6p amino acids 1–213 were nucleotide-free, with intermolecular contacts at the putative GTP-binding site that would prevent nucleotide access. Attempts to cocrystallize Irc6p with GTP, GDP, or nonhydrolyzable analogues were unsuccessful. However, a structural comparison of Irc6p with the nucleotide-binding site of Arl1p cocrystallized with GTP identified several Irc6p residues that might participate in GTP binding (Figure 2, B, D, and E). Lys-22 and Thr-23 correspond to residues in the highly conserved P-loop motif GXXXXGK(T/S) in G domains, although the invariant glycines are absent in Irc6p (Figure 2, B and E). In G domains, the P-loop motif lysine and threonine are involved in binding to the β and γ phosphates of the nucleotide (Panic *et al.*, 2003; Donaldson and Jackson, 2011; Wittinghofer and Vetter, 2011). Specificity for GTP/GDP is typically dependent on conserved asparagine and aspartate residues in a consensus sequence NKXD that interact with the guanine base (Wittinghofer and Vetter, 2011). Irc6p has a suitably positioned glutamate (E121) in a related motif, NVNE (Figure 2, B and E).

We tested wild-type and mutant forms of Irc6p for binding to [^{35}S]GTPγS, using a standard filter-binding assay. In contrast to Arf1p, recombinant full-length Irc6p or the N-terminal domain (aa 1–213) did

	Native Irc6p	Peak (SeMet Irc6p)
Data collection		
Beamline	APS ID24-C	
Detector	ADSC Quantum Q315R	
Wavelength (Å)	0.9795	0.9793
Data processing	HKL	HKL
Space group	$P6_5$	$P6_5$
Unit cell parameters *a*,*b*,*c* (Å); α,β,γ (°)	*a* = 61.638 *b* = 61.638 *c* = 95.144 α = 90.0 β = 90.0 γ = 120.0	*a* = 61.421 *b* = 61.421 *c* = 95.008 α = 90.0 β = 90.0 γ = 120.0
Resolution (Å)	29.32–1.80	35.59–2.05
Number of observations	127,621	137,187
Unique reflections	18,511	25,501
Completeness (%)	97.4 (96.5)	99.3 (99.7)
R-merge (%)[a]	6.6 (54.1)	6.8 (39.8)
<I/σ(I)>	24.12 (3.95)	20.57 (4.23)
Number of Se atoms/ asymmetric unit		Two observed of six expected
Refinement statistics		
Resolution (Å)	53.8–1.8	
Number of reflections	17,548	
R_{work}/R_{free} (%)	19.7/21.8	
High-resolution shell	21.9/28.3	
Number of atoms	1538	
Protein	1498	
Water	40	
Average B-factor	19.3	
Wilson plot *B*	15.8	
V_m	2.1	
Estimated solvent content (%)	40.57	
RMS deviations		
Bond lengths (Å)	0.007	
Bond angles (°)	1.053	
Residues in Ramachandran	157	
Most-favored region (%)	94.6	
Additionally allowed (%)	4.8	
Generously allowed (%)	0.6	
Disallowed (%)	0.0	

[a]*R*-merge = merging *R* factor, $(\Sigma_{hkl} \Sigma_i |I_i(hkl) - <I(hkl)>|) / (\Sigma_{hkl} \Sigma_i I(hkl)) \times 100\%$. Last shell SeMet 2.12–2.05 Å; last shell native 1.86–1.80 Å. Values in parentheses correspond to the statistics for the highest resolution.

TABLE 1: Data collection, processing, and refinement statistics.

not bind GTP in the presence (Figure 2F) or absence (unpublished data) of detergent. These findings, and the absence of consensus GTP-binding motifs, indicate that Irc6p is not a typical GTP-binding protein. However, with a sensitive UV cross-linking assay, GTPγS (but not ATPγS) associated with Irc6p but not with an unrelated protein, the lipid phosphatase Sac1p (Figure 2G; unpublished data). Two mutants, K22A and E121Q, engineered to disrupt putative GTP-binding residues, exhibited substantially reduced cross-linking to GTPγS (Figure 2G). Additionally, production of a stable C-terminally truncated fragment (residues 1–213) by limited proteolysis was slowed in the presence of GMPPNP (Figure S2B), suggesting that Irc6p may be stabilized by nucleotide.

K22A or E121Q mutations were introduced into the genomic *IRC6* locus and crossed into *chc1-ts* or *chs6*Δ strains. The GTP-binding mutants, expressed at wild-type levels (Figure S2C), did not cause defects in either strain with the standard growth assays (Figure 2, H and I). Only at high concentrations of CCFW did the mutations impair growth of the *chs6*Δ cells, but not to the extent of *irc6*Δ (Figure 2I). These findings sharply contrast with the effects of altering cognate P-loop–motif lysines in yeast Arf1p and the rab Ypt1p, which yielded severe phenotypes equivalent to complete gene inactivation (Wagner *et al.*, 1987; Click *et al.*, 2002). Thus the N-terminal domain of Irc6p differs from conventional G domains, neither binding GTP with low micromolar affinity nor exhibiting strong functional defects when mutated to prevent GTP binding.

Irc6p and p34 are members of a conserved protein family

Irc6p shares 15% sequence identity and 41% similarity with human p34. Homology-based structure-modeling programs Phyre, SWISS-MODEL, and ESyPred3D (Lambert *et al.*, 2002; Kelley and Sternberg, 2009; Kiefer *et al.*, 2009) predicted an N-terminal fold for p34 with the same topology as that of Irc6p (Figure S3A). Remarkably, expression of p34 from a multicopy plasmid completely rescued growth defects due to *irc6*Δ in either *chc1-ts* cells or in *chs6*Δ cells on CCFW (Figures 3, A and B, and S3B), revealing an unexpectedly strong functional conservation between Irc6p and p34 despite low sequence homology. Consistent with conserved function, p34 interacts with yeast AP-1 and AP-2 (Figure S3C).

A search of the Conserved Domain Database (CDD; Marchler-Bauer *et al.*, 2011) with the Irc6p sequence did not reveal the N-terminal G-like domain but did indicate a putative conserved domain in the C-terminal region (aa 162–232) that was also present in p34 (*E* value: 2.39e-07). The C-terminal region is designated as an adaptin-binding domain, although no analysis of adaptin binding by the domain has been reported. The CDD identified an additional ≈200 nonredundant eukaryotic protein sequences with putative adaptin-binding domains and, strikingly, 38 with N-terminal P-loop nucleoside triphosphate hydrolase (NTPase) domains and C-terminal adaptin-binding domains (Supplemental Table S1). G domains are a subset of P-loop NTPase domains. Among those with NTPase domains are p34 from rats, as well as sequences from humans and fish, amoeba, and plant species (Figure 4A). Some species encoded more than one Irc6-related protein. In many cases, the sequences delineated as P-loop NTPase were shorter than expected for a full Rossmann fold. A set of eight protein sequences from the 38 predicted two-domain proteins were submitted to the SWISS-MODEL three-dimensional modeling program. In every case, Rossmann fold–like domains consisting of a core of β-strands flanked by α-helices were predicted for the N-terminal regions (two examples are presented in Figure 4B). No models were predicted for the C-terminal "adaptin-binding" regions. Combined with our structural characterization of the N-terminal G-protein fold in Irc6p,

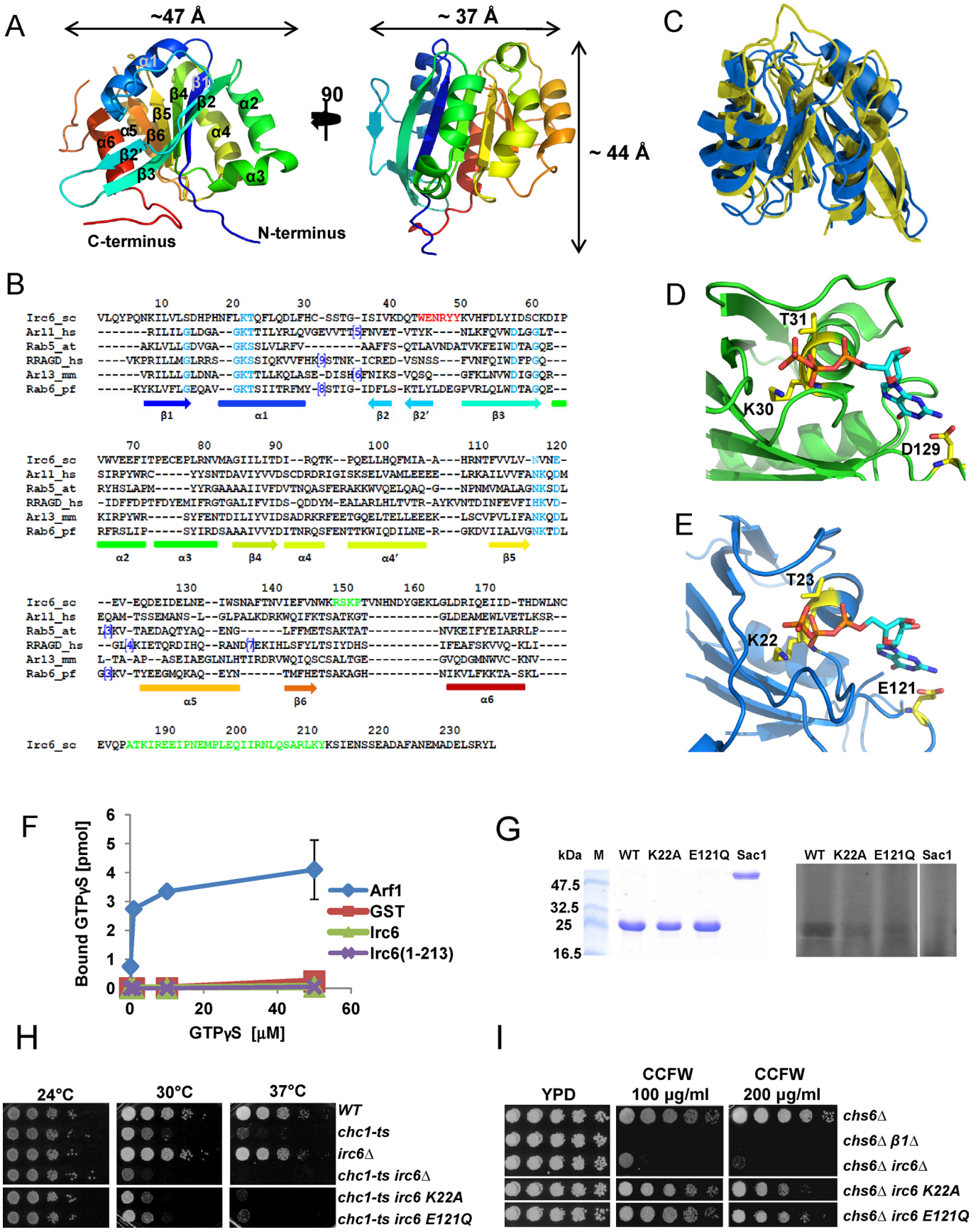

FIGURE 2: A G-like domain in Irc6p. (A) Ribbon representation of Irc6p amino acids 1–213 derived from the crystal structure determined at 1.8 Å resolution. Two perspectives are presented, rotated by 90°. Ribbon is colored in rainbow from blue at the N-terminus to red at the C-terminus, with secondary structure elements numbered. (B) Structure-based

these observations define Irc6p and p34 as founding members of a novel G protein–like family distinguished by an N-terminal G-like domain and a C-terminal region related to p34.

Sequence alignment of the 38 predicted two-domain proteins uncovered a conserved motif with the consensus sequence (I/L)(N/D)(N/T)(R/K)YY located in the accessible loop connecting β2 and β3 strands in Irc6p and the predicted p34 structure (Figure 4, C and D, and Table S1). The motif is not present in the structurally similar G proteins identified in the Dali server search (Figure 2B, motif highlighted in red). As such, the sequence appears to constitute another signature for this group of proteins. We term this motif BC-YY for the beta-strand connecting YY motif. Mutation of the BC-YY motif (YY to AA) compromised function of both Irc6p and p34 (Figure 3C). On the basis of the conservation of this motif, we suggest naming the group of Irc6p/p34-related proteins "BYGR" for BC-YY G-protein related.

The CCD search did not detect the N-terminal P-loop NTPase domain in Irc6p and consequently classified Irc6p as one of the ≈200 sequences without an N-terminal NTPase-like domain. Thus it is likely that additional members of the BYGR family are present in this set of sequences. Indeed, of the sequences with a predicted "adaptin-binding" domain but no predicted G-protein fold, ~80% carry versions of the BC-YY motif.

Our analysis suggests that Irc6p is organized into at least two regions, an N-terminal G-like domain and a conserved C-terminal region. To determine the effects of deleting one of the regions, we designed C- or N-terminal truncations based on the Irc6p structure. When combined with *chs6*Δ, deletion of the C-terminal region (aa 180–237; *irc6*Δ*C*) debilitated growth on CCFW more severely than full deletion of *IRC6*, even at very low CCFW concentrations (Figure 3D). This suggests that, in the absence of the C-terminal region, the G-like domain acts to inhibit Chs3p traffic between the TGN and endosomes, perhaps by nonproductive binding to a normal interaction partner. In a reciprocal experiment, expression of just the Irc6p C-terminal sequences (aa 179–237) partially complemented the growth defect in *chs6*Δ *irc6*Δ cells (Figure 3D). Similar results were obtained with p34 N- and C-terminal regions, although the growth effects were less pronounced than observed with Irc6p (Figure 3D). These results support the functional significance of the two-region model for Irc6p/p34.

Irc6p interacts with proteins involved in TGN/endosome traffic

We identified Irc6p-binding proteins by affinity chromatography of yeast lysate and mass spectrometry, yielding the known interactors AP-1 and AP-2, as well as novel binding partners Ypt31p and Sec4p. Sec4p and Ypt31p are Rab GTPases that function in secretory vesicle traffic between the TGN and the plasma membrane (Novick *et al.*, 1980; Benli *et al.*, 1996; Jedd *et al.*, 1997). In addition, Ypt31p functions in transport between the TGN and endosomes (Chen *et al.*, 2005, 2011). Irc6p interactions with AP-1, AP-2, Ypt31p, and Sec4p were also detected by immunoblotting of proteins isolated by Irc6p affinity chromatography (Figure 5A) and by coimmunoprecipitation of tagged Irc6p expressed from the native chromosomal locus (Figure 5B). Supporting the specificity of these interactions, Irc6p did not bind to the Arf1p GTPase or the Gga2p clathrin adaptor by affinity chromatography nor did it bind to the Rab Ypt1p by coimmunoprecipitation (Figure 5, A and B).

We tested whether purified Ypt31p and Irc6p interact directly. In the presence of GDP, Irc6p did not bind to glutathione *S*-transferase (GST)-Ypt31p (Figure 5C, lanes 5 and 6). Preincubation with a nonhydrolyzable GTP analogue, GMPPNP, stimulated Irc6p binding to GST-Ypt31p but not to GST (Figures 5C, lanes 7 and 9, and S3D). The stimulatory effect of GMPPNP still occurred when the GTP binding–defective Irc6p K22A mutant was tested for Ypt31p binding (Figure 5C, lane 10). This observation suggests that the nucleotide acts on Ypt31p to enhance the interaction. Our results establish that Irc6p binds directly to the activated form of Ypt31p.

Functional interaction of Irc6p with Ypt31p

Double mutant analysis was used to probe functional interactions between Irc6p and Ypt31p or Sec4p in vivo. No enhancement of growth defects was observed when *irc6*Δ was combined with the temperature-sensitive *sec4-8* allele, even at the semipermissive temperature of 30°C (Figure 6A). The absence of genetic interactions at

sequence alignment of Irc6p with similarly folded proteins identified by the Dali server. PDB codes of sequences are 1upt (Arl1), 2efh (Rab5), 2q3f (RRAGD), 3bh7 (Arl3), and 1d5c (Rab6). sc, *Saccharomyces cerevisiae*; hs, *Homo sapiens*; at, *Arabidopsis thaliana*; mm, *Mus musculus*; pf, *Plasmodium falciparum*. Conserved G-protein motifs G1, G3, and G4 are highlighted in light blue. Residues corresponding to the BC-YY motif [(L/I)(N/D)(N/T)(K/R)YY] present in the Irc6p family are in red. Residues that were present in the crystallized Irc6p construct, but lacked any electron density, are green. Dashes either correspond to residues missing in the electron density maps or gaps in the alignment. Numbers in brackets represent residues omitted to facilitate presentation of the alignment. Numbered secondary structure elements (strands β_1–β_6 and helices α_1–α_6) correspond to those shown in (A). (C) Superposition of Irc6p and atRab5. Structures of Irc6p (aa 8–177, blue) and atRab5p (aa 8–172, 2efh, gold) were superimposed with a root mean-square deviation of 2.6 Å using the program COOT (Emsley and Cowtan, 2004; Langer *et al.*, 2008). (D) GTP-binding site of Arl1 with GTP (PDB ID: 1upt). Amino acid side chains involved in GTP binding and conserved in Irc6p are shown in yellow. (E) Putative nucleotide-binding pocket in Irc6p. GTP was modeled into the Irc6p structure using the program COOT (Emsley and Cowtan, 2004). The highly conserved residues involved in GTP-binding are highlighted in yellow. (F) Irc6p does not bind GTP with high affinity. The indicated recombinant proteins (0.5 μM) were incubated with increasing concentrations of ^{35}[S]GTPγS, and bound nucleotide was measured by filter binding and rapid filtration. (G) Irc6p binds GTP by cross-linking. Purified recombinant wild-type Irc6p (WT), Irc6p K22A, and E121Q mutants and Sac1p were incubated with ^{35}[S]GTPγS, subjected to UV illumination, and analyzed for bound nucleotide by SDS–PAGE and autoradiography. Proteins were stained with Coomassie Blue (left panel) or subjected to autoradiography (right panel). M, molecular weight standard (kDa). (H) Effects of Irc6p GTP-binding mutations on *chc1-ts* cell growth. Wild-type (WT, SEY6210), *chc1-ts* (GPY1064), *irc6*Δ (GPY4986), *chc1-ts irc6*Δ (GPY3986), *chc1-ts irc6-K22A* (GPY4988), and *chc1-ts irc6-E121Q* (GPY4989) strains were analyzed for growth, as in Figure 1A. (I) Effects of Irc6p GTP-binding mutations on *chs6*Δ cell sensitivity to CCFW. *chs6*Δ (GPY3102), *chs6*Δ *β1*Δ (GPY3103), *chs6*Δ *irc6*Δ (GPY4042), *chs6*Δ *irc6-K22A* (GPY4990), and *chs6*Δ *irc6-E121Q* (GPY4991) cells were tested for sensitivity to the indicated concentrations of CCFW, as in Figure 1D.

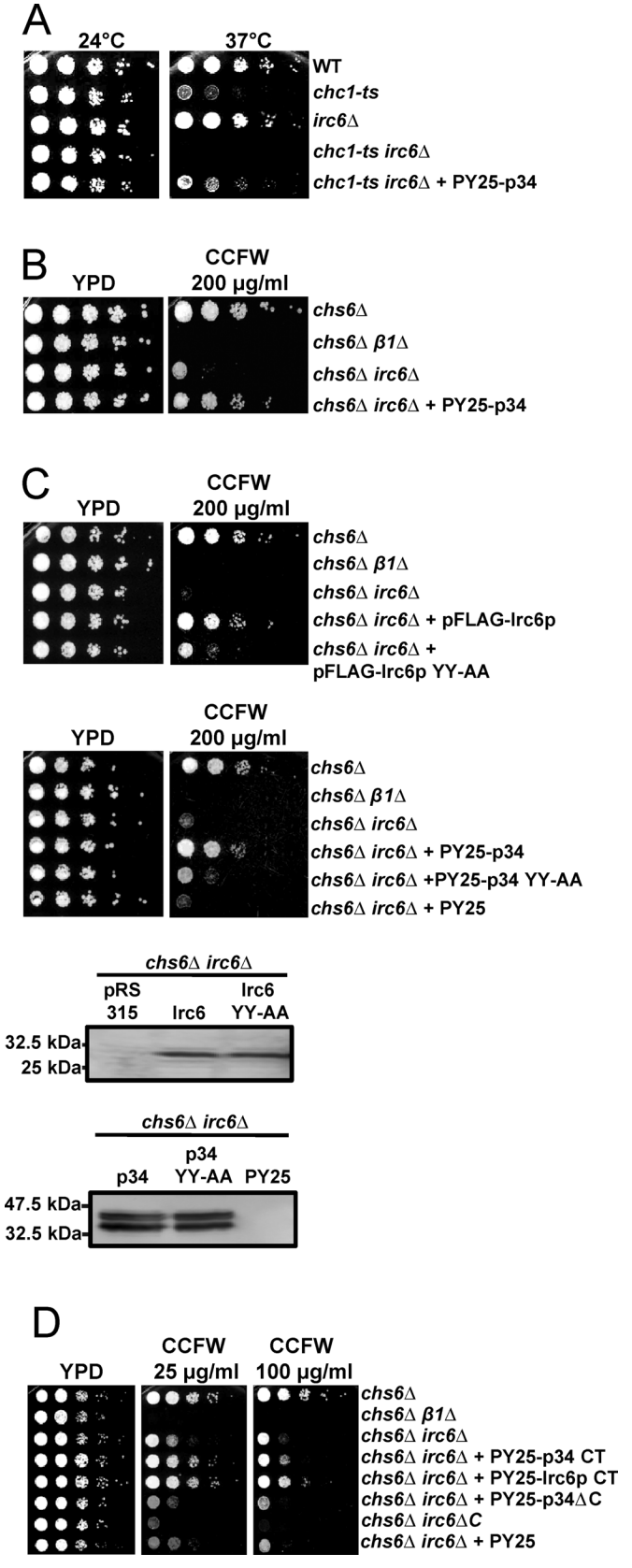

FIGURE 3: Mammalian p34 substitutes for Irc6p in vivo. (A) Indicated strains as in Figure 1A and *chc1-ts irc6*Δ cells expressing 6xHis-tagged p34 from a multicopy plasmid (PY25-p34, GPY5010) were assayed for growth, as in Figure 1A. (B) Indicated strains as in Figure 1D and *chs6*Δ *irc6*Δ cells expressing 6xHis-tagged p34 from a multicopy plasmid (PY25-p34, GPY5011) were assayed for sensitivity to CCFW, as in Figure 1D. (C) Indicated strains as in Figures 1D and 3B and *chs6*Δ *irc6*Δ cells expressing either pFLAG-Irc6p YY-AA (GPY5026) or PY25-p34 YY-AA (GPY5028) were assayed for sensitivity to CCFW, as in Figure 1D. Bottom panels show expression levels of wild-type and YY-AA mutants of Irc6p and p34 from the indicated strains detected by SDS–PAGE and immunoblotting of cell lysates. (D) *chs6*Δ (GPY3102), *chs6*Δ *β1*Δ (GPY3103), *chs6*Δ *irc6*Δ (GPY4042), *chs6*Δ *irc6*Δ expressing the p34 C-terminal region from a multicopy plasmid (PY25-p34 CT, GPY5014), *chs6*Δ *irc6*Δ expressing the Irc6p C-terminal region from a multicopy plasmid (PY25-Irc6p CT, GPY5015), *chs6*Δ *irc6*Δ expressing the p34 N-terminal region from a multicopy plasmid (PY25-p34ΔC, GPY5016), and *chs6*Δ *irc6*ΔC (GPY4993) were tested for sensitivity to the indicated concentrations of CCFW, as in Figure 1D.

any of the tested temperatures suggests that Irc6p does not functionally interact with Sec4p in secretory vesicle traffic, so this interaction was not further investigated.

Ypt31p and the related Ypt32p constitute a redundant pair of Rab GTPases that function in both secretory vesicle transport and traffic between the TGN and endosomes (Benli *et al.*, 1996; Jedd *et al.*, 1997; Ortiz *et al.*, 2002; Chen *et al.*, 2005, 2011; Sciorra *et al.*, 2005; Furuta *et al.*, 2007). Deletion of either Ypt does not cause overt growth defects, but deletion of both is lethal (Benli *et al.*, 1996; Jedd *et al.*, 1997). As one test for genetic interactions, we monitored the effect of *irc6*Δ on growth of cells harboring *ypt31*Δ and the temperature-sensitive *ypt32-A141D*^{ts} allele (Jedd *et al.*, 1997). The *ypt31*Δ *ypt32-ts* cells grew normally at 24°C, exhibited slowed growth at the semipermissive temperature of 33°C, and did not grow at 37°C (Figure 6B). Consistent with function of Irc6p with Ypt31/32p, *irc6*Δ dramatically inhibited the growth of *ypt31*Δ *ypt32-ts* cells at 33°C but did not affect growth at 24°C or at any temperature when present by itself or in combination with only *ypt31*Δ (Figure 6B).

We applied the CCFW assay to mutant combinations with *chs6*Δ to distinguish between Irc6p roles with Ypt31/32p in the secretory pathway or TGN-endosome traffic. In *chs6*Δ cells, increased sensitivity to CCFW reflects a redistribution of Chs3p from the TGN-endosome cycling pathway to the plasma membrane (Valdivia *et al.*, 2002; Copic *et al.*, 2007). Because Chs3p transport to the plasma membrane requires a functional secretory pathway, increased CCFW sensitivity in *chs6*Δ cells can be attributed to effects on TGN-endosome traffic. At 24°C, *ypt31*Δ *ypt32-ts* sensitized *chs6*Δ cells to CCFW more than *irc6*Δ, with effects approaching that of AP-1 inactivation (*β1*Δ; Figure 6C), supporting an important role for Ypt31/32p in TGN-endosome cycling of Chs3p. Importantly, *irc6*Δ intensified the sensitivity when introduced into *ypt31*Δ *ypt32-ts chs6*Δ cells, even at a low CCFW concentration (10 μg/ml) at which *irc6*Δ did not have an effect by itself in *chs6*Δ cells (Figure 6C). Similar genetic interactions were observed between *irc6*Δ and *ypt31*Δ in cells expressing the wild-type *YPT32* (Figure 6D). These results provide evidence that Irc6p functions with Ypt31/32p in Chs3p transport between the TGN and endosomes.

Irc6p links Ypt31p to AP-1

To assess the possibility that Irc6p acts to bridge AP-1 and Ypt31p, we determined whether GST-Ypt31p can bind to AP-1 in extracts from *irc6*Δ cells or *irc6*Δ cells expressing FLAG-tagged Irc6p. In cells expressing FLAG-Irc6p, both Irc6p and AP-1 bound to GST-Ypt31p but not to GST (Figure 7A). Low but specific binding to AP-2 was

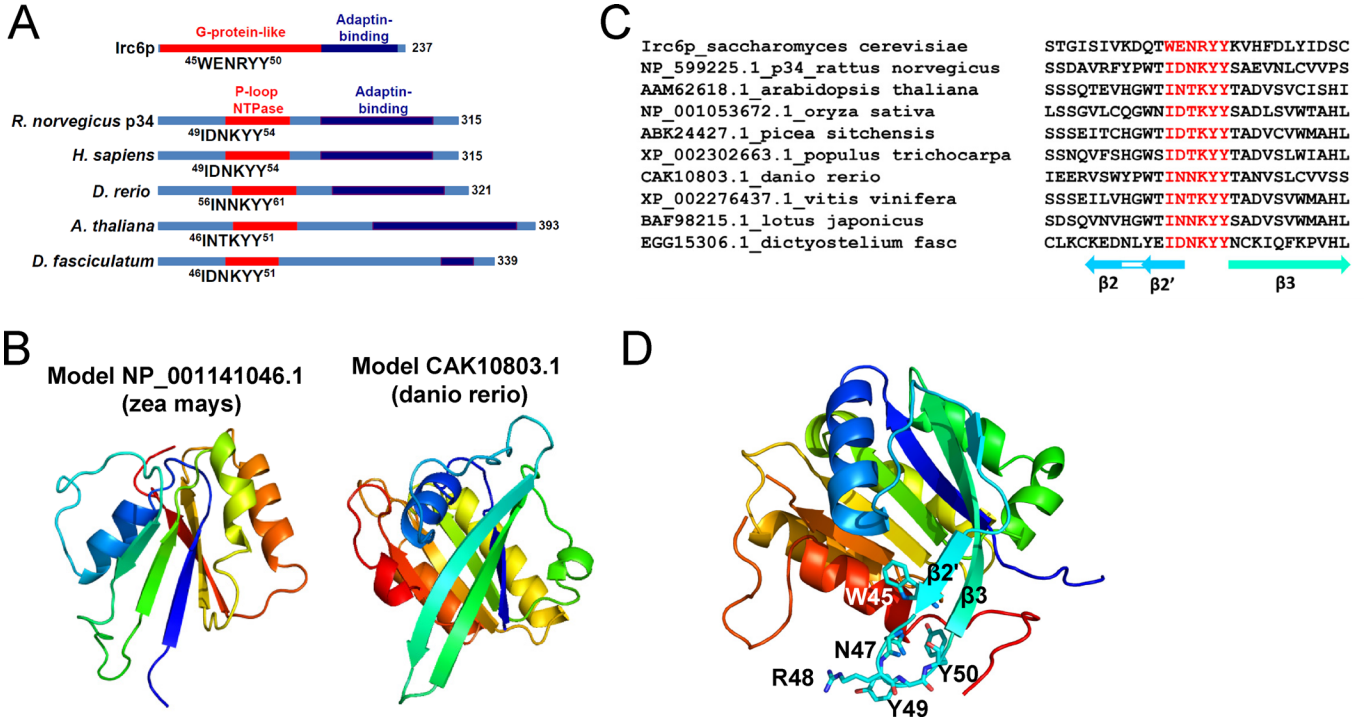

FIGURE 4: The Irc6/p34 G-protein–like family. (A) Diagrams of domain organization and conserved BC-YY motifs in selected members of the family. (B) Predicted three-dimensional structures of Irc6p/p34-related sequences from *Zea mays* and *Danio rerio*. Models were generated by the program SWISS-MODEL, and figures were made with PyMOL. (C) Clustal Omega (www.clustal.org/omega/) alignment of sequences from diverse species belonging to the novel G protein–like family. Highly conserved residues in the sequences corresponding to Irc6p amino acids 34–61 are highlighted in red. (D) Conserved BC-YY motif [(L/I)(N/D)(N/T)(K/R)YY] in Irc6p is localized in loop connecting β_2 and β_3.

also observed. Strikingly, GST-Ypt31p did not bind to AP-1 (or AP-2) in the cell extract lacking Irc6p (Figure 7A), suggesting a role for Irc6p in linking AP-1 to Ypt31p.

Binding of the two Irc6p domains to Ypt31p and AP-1 was also examined. When purified proteins were used, GST-Ypt31p (with GMPPNP) bound both Irc6p N- and C-terminal regions (Figure 7B), with an apparent preference for the C-terminal region. A similar experiment was carried out to assess AP-1 binding, but in this case the Irc6p constructs were used for affinity binding with cell extracts as a source of AP-1. As with Ypt31p, both the Irc6p N- and C-terminal regions bound AP-1, although with somewhat higher levels of AP-1 binding by the N-terminal region (Figure 7C, lanes 3–5). Taken together, the results from both physical and genetic interaction studies suggest that Irc6p and Ypt31/32p act together with AP-1 in TGN-endosome traffic.

DISCUSSION

The number and variety of clathrin coat accessory proteins confer a complexity to CCV formation that distinguishes the process from simpler mechanisms that drive biogenesis of other well-characterized classes of coated vesicles (Kirchhausen, 2000). In this study, we have identified Irc6p as a founding member of a new G protein–like family that functions with AP-1 and Ypt31p in TGN-endosome traffic. These findings define Irc6p and, by extension, its functional mammalian homologue p34, as a novel type of clathrin coat accessory factor.

The crystal structure of Irc6p amino acids 1–185 revealed an N-terminal Rossmann fold that is most similar to small G proteins of the Arf and Rab families. However, Irc6p lacks signature G-protein motifs, and both biochemical and genetic experiments provide evidence that the N-terminal region of Irc6p is not a conventional G domain that relies on GTP binding for function. Instead, our results suggest that low-affinity GTP binding might contribute to Irc6p stability. Even so, the inefficient GTP binding in vitro, the subtle in vivo defects caused by structure-based mutation of candidate GTP-binding residues, and the lack of conservation of those residues in other family members favor a view that GTP binding is not an important feature of the Irc6p/p34 family. In this way, the Irc6p/p34 N-terminal domain may represent a "pseudo-G domain" that has retained protein interaction functions but not nucleotide binding, as has been recently suggested for G-like domains in mammalian AGAP1 and LRRK (Luo *et al.*, 2012).

Our results offer several lines of evidence that Irc6p directly functions in clathrin-mediated transport between the TGN and endosomes. First, Irc6p physically interacts with AP-1 and Ypt31p, both associated with TGN-endosome traffic. Second, *IRC6* deletion affects Kex2p-dependent α-factor maturation in *chc1-ts* cells and Chs3p-dependent CCFW sensitivity in *chs6*Δ cells. Both Kex2p and Chs3p cycle between the TGN and endosomes, and defects in clathrin, AP-1, and clathrin accessory proteins yield phenotypes similar to those observed for *irc6*Δ (Seeger and Payne, 1992; Yeung *et al.*, 1999; Valdivia *et al.*, 2002; Fernandez and Payne, 2006). Third, reduced activity of Ypt31/32p caused CCFW sensitivity in *chs6*Δ cells, and *irc6*Δ enhanced this sensitivity. These results provide evidence that Ypt31/32p are involved in Chs3p cycling between the TGN and endosomes, supporting models for Ypt31/32p function in TGN-endosome traffic derived from defects in transport of other

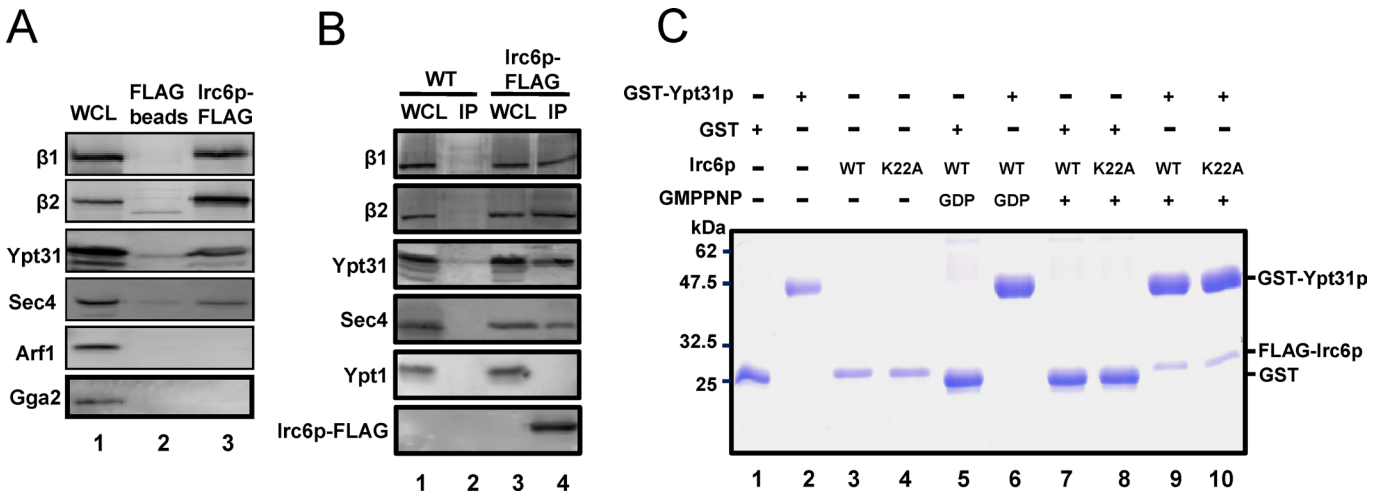

FIGURE 5: Irc6p physically interacts with AP complexes and Rab proteins. (A) Irc6p affinity binding. Purified FLAG-tagged Irc6p bound to FLAG affinity beads or FLAG affinity beads alone were incubated with WCL of wild-type cells (SEY6210). Bound proteins were separated by SDS–PAGE and analyzed using immunoblotting for the indicated proteins. Amount loaded in the WCL lane corresponds to 6% of the lysate used for affinity binding in lanes 2 and 3. (B) Irc6p coimmunoprecipitation. Wild-type cells (WT, SEY6210) or cells expressing Irc6p-FLAG from the endogenous locus (Irc6p-FLAG) were lysed under nondenaturing conditions and incubated with FLAG affinity beads. WCL and immunoprecipitated (IP) proteins were separated by SDS–PAGE and analyzed by immunoblotting for the indicated proteins and FLAG (Irc6p-FLAG). Irc6p-FLAG is difficult to detect in WCL, due to low expression levels. Amount loaded in the WCL lane corresponds to 6% of the lysate used for immunoprecipitation. (C) Direct interaction between Irc6p and Ypt31p. Purified GST (lane 1) or GST-Ypt31p (lane 2) bound to glutathione beads and purified FLAG-Irc6p (WT, lane 3) or FLAG-Irc6p-K22A (lane 4) were combined as indicated (lanes 5–10) with or without preloaded 1 mM GDP (lanes 5 and 6) or 1 mM GMPPNP (lanes 7–10). Protein interaction was analyzed by SDS–PAGE and Coomassie Blue staining. Amount of Irc6p loaded in lanes 3 and 4 corresponds to 40% of the amount used for affinity binding in lanes 5–10.

cargo (Chen *et al.*, 2005, 2011; Furuta *et al.*, 2007). Enhancement of CCFW sensitivity resulting from the combination of *irc6*Δ with *ypt31/32* mutants further supports assignment of Irc6p function to traffic between the TGN and endosomes. In contrast, although Irc6p binds to AP-2, we did not detect effects of *irc6*Δ on AP-2–mediated endocytosis. Thus a role for Irc6p in endocytosis remains to be established.

Like some other trafficking proteins (Borlido *et al.*, 2009), Irc6p has also been implicated in nuclear functions. In one report, *irc6*Δ cells displayed increased levels of recombination protein foci in nuclei, but no defects in recombination were observed (Alvaro *et al.*, 2007). In an independent study, *irc6*Δ was identified in a screen for mutations that reduced DNA double-stranded break healing by telomerase (Zhang and Durocher, 2010). Whether these phenotypes reflect a direct role for Irc6p in the nucleus or result from indirect effects of an Irc6p deficiency is not clear.

Affinity-binding experiments using Ypt31p as bait suggest that Irc6p can link Ypt31p to AP-1. Additionally, stimulation of Irc6p binding to a GTP analogue–activated form of Ypt31p indicates that Irc6p is an effector of Ypt31p. We envision that the ability of Irc6p to bind to AP-1 and serve as a Ypt31p effector provides a mechanism to bring together AP-1 and activated Ypt31p in forming CCV. CCV-associated Ypt31p could then recruit additional effectors, as has been observed for other Rab proteins (Hutagalung and Novick, 2011; Segev, 2011). In this way, Irc6p would function to expand the repertoire of coat-associated proteins during biogenesis of AP-1 clathrin coats. Whether Irc6p directly links AP-1 and Ypt31p or acts with a separate linking protein(s) will require additional investigation. The less-severe effects of *irc6*Δ compared with inactivation of AP-1 or Ypt31/32p likely reflect redundant or alternative mechanisms that can more effectively accommodate the absence of Irc6p function than a loss of the core transport functions of AP-1 or Ypt31/32p.

Results from both structural and functional analyses support a bipartite model for Irc6p organization: the N-terminal G protein–like domain and a conserved C-terminal region. Of note, the conserved C-terminal domain predicted by the CCD overlaps with the final α-helix of the G-like domain (aa 166–175). The observation that amino acids 166–175 constitute the final helix in the G-like domain crystal structure suggests that these sequences are not part of an independent C-terminal domain. Furthermore, a C-terminal fragment (aa 180–237) that does not include the final G-like domain helix was able to substitute for full-length Irc6p in vivo, indicating that amino acids 166–179 are not essential for function of the C-terminal region. On the basis of these results, we consider the conserved C-terminal region as a separate "domain" beginning after the final helix of the G-like domain. Sequences following amino acid 186 were not detected in the Irc6p crystal, leaving the structural organization of the C-terminal region unclear. Secondary-structure prediction algorithms suggest two α-helical regions between amino acid 199 and the C-terminus, as well as the possibility of a coiled coil between amino acid 199 and amino acid 212 (Figure S3E). It appears unlikely that the putative coiled coil mediates homo-dimerization, since there was no significant difference in gel filtration elution profiles of recombinant full-length Irc6p and an Irc6p fragment lacking amino acids 190–237 (unpublished data). Additional experiments will be needed to determine the structure of the C-terminal region and define the structural arrangement of the N- and C-terminal regions in full-length Irc6p.

Although the C-terminal region is designated as an "adaptin-binding domain" in the CCD database, our results indicate that both the N-terminal and C-terminal regions have the capacity to bind

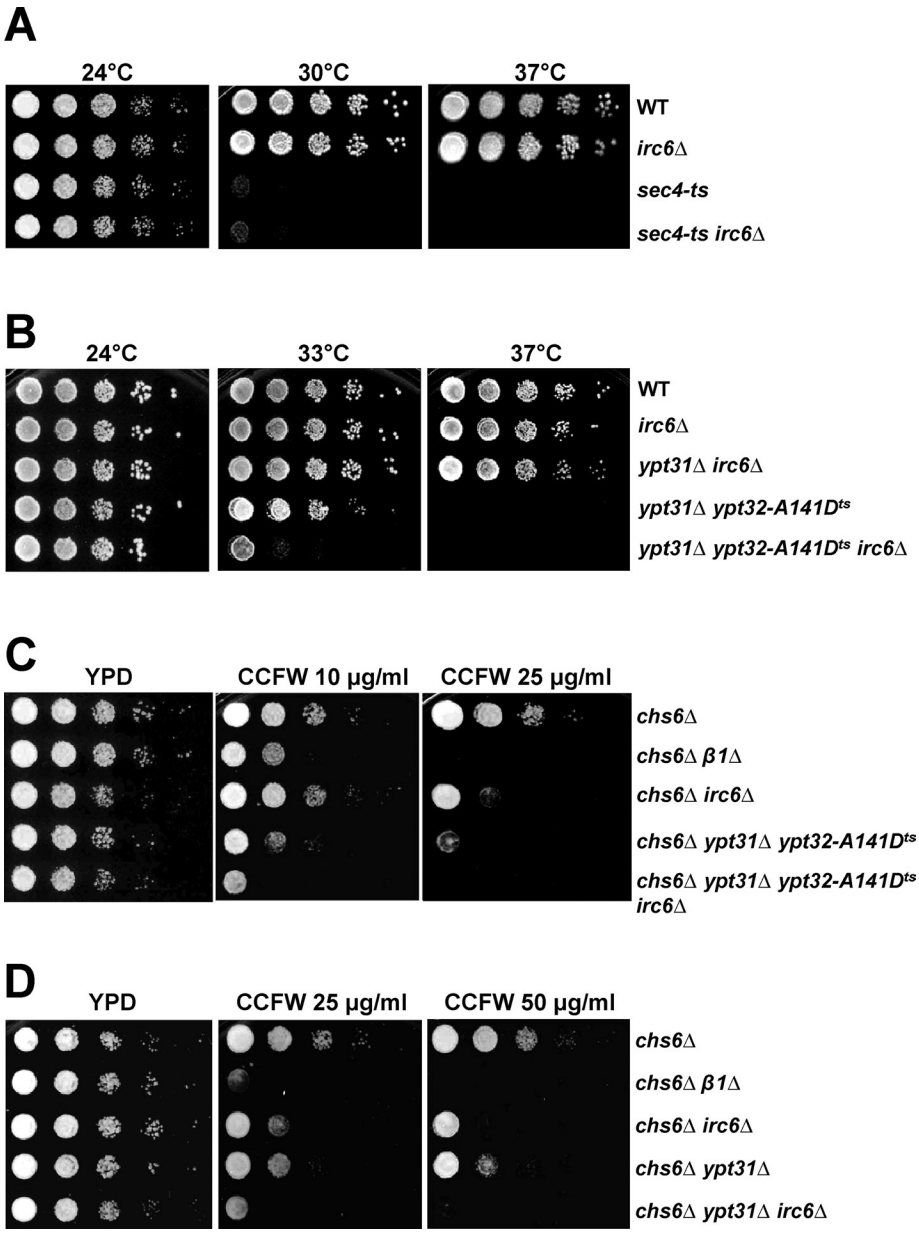

FIGURE 6: Irc6p functionally interacts with Ypt31p. (A) Absence of genetic interaction between *irc6*Δ and *sec4* by growth. Wild-type (WT, SEY6210), *irc6*Δ (GPY4986), *sec4-8* (*sec4-ts*, NY28), and *sec4-8 irc6*Δ (GPY4994) cells were analyzed for growth at the indicated temperatures, as in Figure 1A. (B) Genetic interaction between *irc6*Δ and *ypt31/32*^{ts} by growth. Wild-type (WT, SEY6210), *irc6*Δ (GPY4986), *ypt31*Δ *irc6*Δ (GPY4972-4D), *ypt31*Δ *ypt32-A141D*^{ts} (GPY4972-6D), and *ypt31*Δ *ypt32-A141D*^{ts} *irc6*Δ (GPY4972-7D) cells were analyzed for growth at the indicated temperatures, as in Figure 1A. (C) Genetic interactions between *ypt31/32*^{ts} and *irc6*Δ by CCFW sensitivity. *chs6*Δ (GPY3102), *chs6*Δ *β1*Δ (GPY3103), *chs6*Δ *irc6*Δ (GPY4042), *chs6*Δ *ypt31*Δ *ypt32-A141D*^{ts} (GPY4985-51C), and *chs6*Δ *ypt31*Δ *ypt32-A141D*^{ts} *irc6*Δ (GPY4985-8B) cells were tested for their sensitivity to the indicated concentrations of CCFW, as in Figure 1D. (D) Genetic interactions between *irc6*Δ and *ypt31*Δ by CCFW sensitivity. Strains as in Figure 6C plus *chs6*Δ *ypt31*Δ (GPY4985-79D) and *chs6*Δ *ypt31*Δ *irc6*Δ (GPY4985-6A) were assayed as in Figure 1D.

AP-1 and Ypt31p. However, the different functional consequences observed when the domains were expressed separately imply that the binding modes of the two Irc6p regions to AP-1 and Ypt31p are distinct. The ability of the C-terminal domain to bind both AP-1 and Ypt31p suggests that this domain can partly reinstate the functional interactions mediated by the full-length protein, thereby accounting for partial complementation when the C-terminal domain is expressed by itself in *irc6*Δ cells. In contrast, expression of the N-terminal domain alone was more deleterious than the complete absence of Irc6p. This finding can be explained by nonproductive, inhibitory binding of the N-terminal domain to AP-1 and/or Ypt31/32, since mutations in either of these factors yields more severe phenotypes than deletion of *irc6*Δ.

Complete complementation of *irc6*Δ growth defects by expression of full-length mouse p34 and the interaction of p34 with yeast AP-1 revealed a surprisingly strong degree of functional conservation between the yeast and mouse proteins, thereby suggesting a role for mammalian p34 in AP-1–dependent TGN-endosome traffic. The functional similarities between yeast and human proteins are likely to reflect a conserved two-region structure. Modeling algorithms predicted a Rossmann fold for the N-terminal domain of p34 similar to that of Irc6p. Database searches also predict common C-terminal regions in Irc6p and p34. Importantly, expression of the p34 C-terminal region in *irc6*Δ cells mimicked the growth-enhancing effects of the C-terminal Irc6p region. The presence of sequences encoding proteins with the same predicted domain arrangement and the conserved BC-YY motif in organisms as diverse as fungi, mammals, and plants suggest that the functions of Irc6p andp34 have been broadly conserved in evolution. On the basis of these findings, we propose that Irc6p/p34 are founding members of a previously unrecognized family related to small G proteins, constituting a novel class of conserved clathrin coat accessory factors.

MATERIALS AND METHODS

Plasmids and yeast strains

For generation of recombinant 6xHis- or FLAG-tagged Irc6p fusion proteins, DNA encoding Irc6p was amplified by PCR from yeast genomic DNA. Products were cloned in-frame into the *Nco*I/*Xho*I sites of pET-28a or the *Nco*I/*Nde*I sites of pET-15b bacterial expression vectors for 6xHis- or FLAG-tagged constructs, respectively. For generation of FLAG-Irc6p for expression in yeast, the FLAG tag was encoded in the forward primer used in PCR, such that the protein contained the sequence MGDYKDDDDKSG directly fused to Irc6p. The resulting PCR product was cloned into the *Xba*I/*Not*I sites of centromeric plasmid pRS315 containing the *PRC1* promoter and *CYC1* terminator region, and into the *Xho*I/*Bam*HI sites of multicopy PY25 containing the glyceraldehyde-3-phosphate dehydrogenase promoter (Li *et al.*, 2008). DNA encoding p34 full-length, its N-terminal–region amino acids 1–179, or the C-terminus amino acids 158–315 was amplified by PCR using mouse

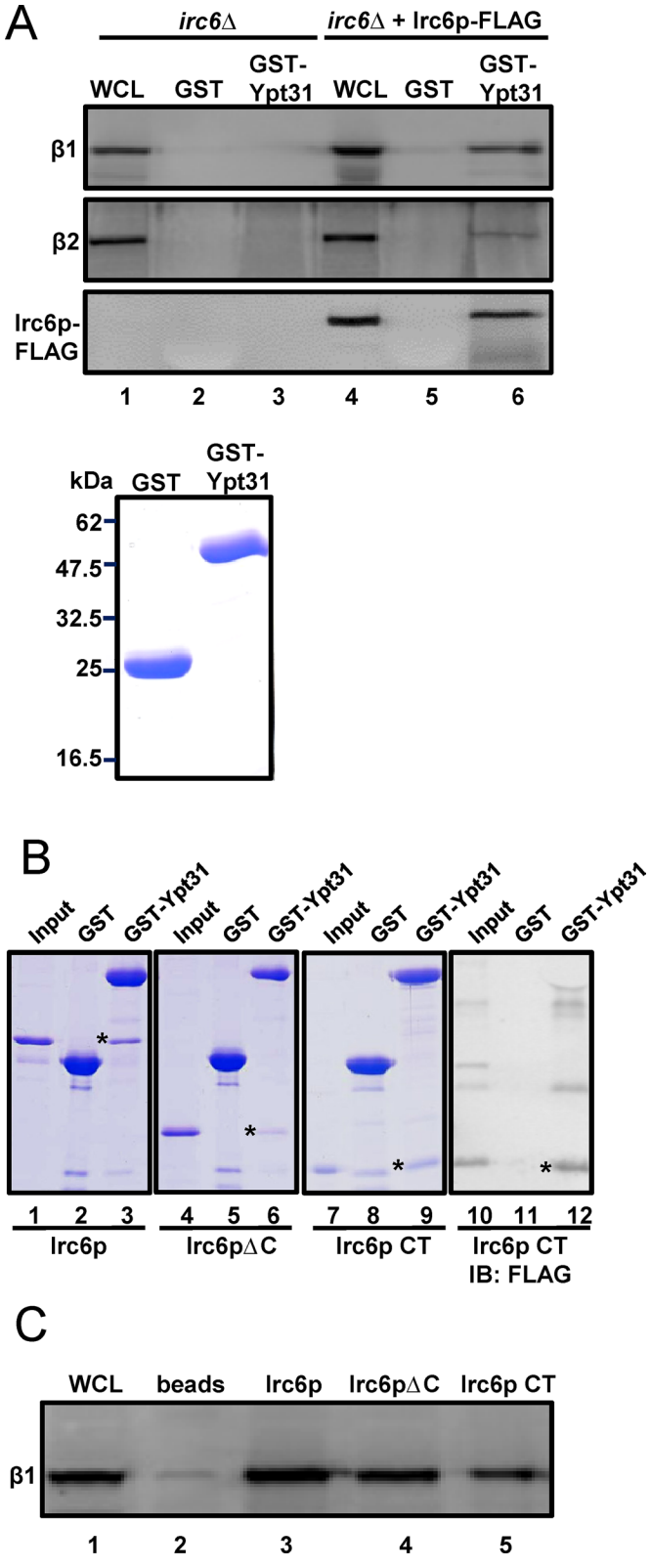

FIGURE 7: Irc6p links Ypt31p to AP-1. (A) Irc6p is necessary for Ypt31p binding to AP-1. GST or GST-Ypt31p bound to glutathione-Sepharose (bottom panel, Coomassie Blue–stained) was incubated with WCL (lanes 1 and 4) from *irc6*Δ cells (GPY4986, lanes 2 and 3) or *irc6*Δ cells expressing FLAG-Irc6p (GPY5018, lanes 5 and 6). Bound proteins were eluted, separated by SDS–PAGE, and analyzed by immunoblotting for β_1, β_2, and FLAG (top panel). (B) Ypt31p interacts with Irc6p N- and C-terminal regions. FLAG-tagged Irc6p constructs indicated at the bottom of each panel were incubated with GST or GST-Ypt31p bound to glutathione-Sepharose (in the presence of 1 mM GMPPNP). Irc6p constructs alone (input) or proteins associated with GST or GST-Ypt31p were separated by SDS–PAGE and either stained with Coomassie Blue (left three panels) or subjected to immunoblotting with FLAG antibody (right-most panel). Asterisk in each panel indicates Irc6p or Irc6p fragment associated with GST-Ypt31. (C) AP-1 interacts with N- and C-terminal regions of Irc6p. FLAG-Irc6p constructs used in (B) were bound to FLAG-affinity beads and incubated with WCL (lane 1) of wild-type cells SEY6210. Proteins associated with FLAG beads only (lane 2), wild-type FLAG-Irc6p (Irc6p, lane 3), FLAG-Irc6pΔC (lane 4) or FLAG-Irc6pCT (lane 5) were eluted, separated by SDS–PAGE, and analyzed by immunoblotting for β_1.

cDNA reverse-transcribed from 1 μg of RNA extracted from the mouse V6.5 embryonic stem cell line. For expression in yeast, p34 constructs were cloned into the *Xho*I/*Bam*HI sites of PY25, and for expression in *Escherichia coli*, p34 was cloned into the pET-15b vector using the *Nde*I and *Bam*HI sites. Irc6p K22A and E121Q mutations were introduced by site-directed mutagenesis of pET28a or pET-15b constructs using the QuikChange system (Stratagene, LalJolla, CA). All constructs were verified by sequencing.

For introduction of point mutations into endogenous *IRC6*, *irc6-K22A*, irc6-*E121Q*, or *irc6-Y49A Y50A* (YY-AA) in pET-15b was used as a template for PCR. The resulting products were cotransformed with pRS313 (*HIS3*; Sikorski and Hieter, 1989) into GPY4986. His+ colonies were replica-plated onto agar medium containing 5-fluoroorotic acid to identify cells in which the mutant sequences replaced *URA3*. C-terminal truncation (*irc6ΔC*; aa 1–179) and C-terminal tagging of Irc6p in the genomic locus were performed as described in Longtine *et al*. (1998), using the vector pFA6a-FLAG-TRP1. All alterations of genomic *IRC6* were verified by PCR and sequencing, and protein expression was evaluated by immunoblotting.

Double mutant strains were generated by standard yeast mating, sporulation, and isolation of haploid segregants. The genotypes of all strains used in this study are listed in Table S2.

Yeast media, growth assays, radiolabeling and immunoprecipitation, and fluorescence microscopy

Strains were grown in YPD (1% Bacto yeast extract [Difco, Detroit, MI], 2% Bacto peptone [Difco], 2% dextrose) or SD media (0.67% yeast nitrogen base without amino acids [Difco], 2% dextrose) with the appropriate supplements. CCFW (Sigma-Aldrich, St. Louis, MO) was added to YPD agar plates at the concentrations indicated in the figures. For growth tests, cells were diluted to 1×10^7 cells/ml and then serially diluted 10-fold before dilutions were spotted onto appropriate agar plates. K28 toxin sensitivity was assayed as described in Carroll *et al*. (2009). Radiolabeling and immunoprecipitation of α-factor was performed as described previously (Fernandez and Payne, 2006). CCFW bud-scar staining was carried out as described in Duncan *et al*. (2007).

Protein purification

For biochemical studies, pET-15b or pET-28a containing 6xHis- or FLAG-tagged Irc6p constructs were transformed into *E. coli* BL21(DE3). Protein expression was induced with 0.4 mM isopropyl β-D-1-thiogalactopyranoside (IPTG) at 0.8 OD_{600}, and cells were grown at 24°C overnight in either Luria–Bertani broth (LB) medium or M9 medium substituted with seleno-methionine. Cells were resuspended in lysis buffer (25 mM Tris–HCl, pH 7.5, 150 mM NaCl,

5% glycerol, 2 mM $MgCl_2$, 0.5% n-octyl-β-D-glucopyranoside, and protease inhibitor cocktail without EDTA [Roche Diagnostics GmbH, Mannheim, Germany]), lysed by sonication, and subjected to centrifugation at 20,000 × *g* for 30 min. 6xHis- or FLAG-tagged proteins in the soluble fraction were bound to Ni-NTA Superflow beads (Qiagen GmbH, Hilden, Germany) or anti-FLAG M2 affinity beads (Sigma-Aldrich), respectively. Beads were washed with buffer S (25 mM Tris–HCl, pH 7.5, 150 mM NaCl, 5% glycerol, 2 mM $MgCl_2$), and proteins of interest were eluted with either buffer B (buffer S + 250 mM imidazole) or FLAG elution buffer (buffer S + 150 µg/ml FLAG peptides [Sigma-Aldrich]). For the GTP-binding filter assay, pGex-4T-1, pET22b-Arf1 (Arf1-His6), pET21a-Irc6 (Irc6-His6), and pET28a-Irc6(1-213) (His6-Irc6(1-213)) in BL21(DE3) codon+ bacteria were grown to ~1 OD_{600} at 37°C, and protein expression was induced by 1 mM IPTG for 2 h at 37°C. Cells were resuspended in ice-cold lysis buffer (20 mM HEPES, pH 7.4, 100 mM NaCl, 1 mM EDTA, 2 mM $MgCl_2$, 10 mM imidazole, pH 8, 1 mM dithiothreitol [DTT]) containing 28 µl of protease inhibitor cocktail (Sigma–Aldrich), lysed, and purified as above with Ni-NTA beads or glutathione-Sepharose using elution buffers for Ni-NTA (20 mM HEPES, pH 7.4, 100 mM NaCl, 1 mM EDTA, 2 mM $MgCl_2$, 250 mM imidazole, pH 8, 1 mM DTT) or glutathione-Sepharose (20 mM HEPES, pH 7.4, 100 mM NaCl, 1 mM EDTA, 2 mM $MgCl_2$, 10 mM imidazole, pH 8, 1 mM DTT, 20 mM reduced glutathione). GST, Irc6-His6 and His6-Irc6(1-213), but not Arf1-His6, were dialyzed overnight at 4°C in 20 mM HEPES (pH 7.4), 100 mM NaCl, 1 mM EDTA, 2 mM $MgCl_2$, 1 mM DTT, and 0.5 mM phenylmethylsulfonyl fluoride (PMSF), and were further purified using a Superdex S75/H30 column.

For large-scale purification, cells were resuspended in lysis buffer and lysed using a french press. Soluble proteins were collected after centrifugation at 50,000 × *g* for 30 min. The supernatant was applied to a Ni-NTA Superflow column (Qiagen) previously equilibrated with buffer A (25 mM Tris-HCl, pH 7.5, 150 mM NaCl, 5% glycerol, 2 mM $MgCl_2$, 30 mM imidazole). The column was washed with buffer A, and Irc6p was eluted with a gradient of imidazole in buffer A. The eluted protein pool was loaded onto a HiLoad 16/60 Superdex 200 gel filtration column (GE Healthcare, Uppsala, Sweden) equilibrated in GF buffer (25 mM Tris-HCl, pH 7.5, 150 mM NaCl, 5% glycerol, 2 mM $MgCl_2$). The gel filtration peak was pooled and concentrated using an Amicon Ultra Centrifugal Filter with a 30-kDa cutoff to a final concentration of 12 mg/ml.

Crystallization and structure determination

Crystallization was performed at the University of California at Los Angeles (UCLA) Crystallization Facility using a Mosquito-TTP nanoliter dispenser. Crystals of native Irc6p and its seleno-methionine variant were obtained at 20°C using the hanging-drop vapor-diffusion technique by mixing equal volumes of protein (12 mg/ml) and reservoir solutions (0.2 M ammonium sulfate, 0.1 M MES, pH 6.5, 30% [wt/vol] polyethylene glycol [PEG] monomethyl ether 5000 or 0.2 M ammonium nitrate, pH 6.3, 20% [wt/vol] PEG 3350). Irc6p crystals belonged to the space group $P6_5$, with the following unit-cell parameters: $a = b = 61.6$; $c = 95.1$ Å; one molecule in the asymmetric unit; and an estimated solvent content of ~40.6%. Crystals of native Irc6p diffracted to 1.8 Å, and crystals of SeMet-Irc6p diffracted to 2.3 Å resolution.

Prior to data collection, crystals were frozen in a cryoprotectant consisting of 0.2 M ammonium nitrate (pH 6.3), 20% (wt/vol) PEG 3350, and 25% glycerol.

Data sets were collected at the Advanced Photon Source (Chicago, IL) at beamline 24ID-C. Both native and derivative data sets were processed using the programs Denzo and Scalepack from the HKL program suite (Otwinowski and Minor, 1997). Initial single wavelength anomalous dispersion (SAD) phases were calculated with the SHELXC/D/E and HKL2MAP program suite (Pape and Schneider, 2004; Sheldrick, 2010). Data collection and processing statistics are listed in Table 1. Density modification was performed using the DM program from the CCP4 package. Diffraction data from 27.3 to 1.8 Å were used for refinement and electron density map calculations. Graphic operations and model building were performed with ARP/wARP and COOT (Emsley and Cowtan, 2004; Langer *et al.*, 2008). For refinement and map calculations, REFMAC was used (Emsley and Cowtan, 2004; Vagin *et al.*, 2004). An overall quality factor of 99.4% was obtained using the program Errat2 (Colovos and Yeates, 1993). All structure figures were prepared using PyMOL (DeLano Scientific, San Carlos, CA). The coordinates and structure factors have been submitted to the PDB (www.rcsb.org) with the accession code 3uc9.

GTP-binding assays

The nucleotide-binding assay was performed using the rapid filtration methods described by Randazzo *et al.* (1995). Reactions were carried out in 50 µl of 25 mM HEPES (pH 7.4), 100 mM NaCl, 1 mM EDTA, 0.5 mM $MgCl_2$, 1 mM DTT, 0.1% (wt/vol) sodium cholate, and 3 mM DMPC containing 500 nM of protein and varying concentrations of [^{35}S]GTPγS (~5000 cpm/pmol; Perkin Elmer-Cetus, Boston, MA) for 2 h at 30°C. Reactions were stopped by addition of 2 ml of ice-cold TNMD buffer (25 mM Tris, pH 7.4, 100 mM NaCl, 10 mM $MgCl_2$, 1 mM DTT) and passed through BA85 filters (Millipore, Billerica, MA) using a vacuum manifold. Filters were washed with ice-cold TNMD and dried, and radioactivity was determined by scintillation counting. For cross-linking, 1 µg purified protein was incubated with 25 µCi of [^{35}S]GTPγS (Perkin Elmer-Cetus) in 50 µl reaction buffer (50 mM Tris-HCl, pH 7.5, 150 mM NaCl, 0.1% Triton X-100, 0.2 mM EDTA, 10 mM $MgCl_2$, 1 mM DTT, 10 µg/ml bovine serum albumin) in a 96-well plate placed on ice. A handheld UV lamp was placed directly on the 96-well plate, and samples were irradiated for 30 min at 254 nm. Samples were analyzed by SDS–PAGE and autoradiography.

Protein interaction studies

For obtaining whole-cell lysates (WCL), cells were converted to spheroplasts, resuspended in buffer Y (50 mM HEPES, pH 6.9, 100 mM NaCl, 1 mM $CaCl_2$, 2 mM $MgCl_2$, 2% glycerol, 0.8% n-octyl-β-D-glucopyranoside) containing protease inhibitor cocktail (Sigma-Aldrich), and lysed by agitation with glass beads. Lysates were subjected to centrifugation at 4°C for 25 min at 20,000 × *g*.

For affinity-binding studies, WCL corresponding to lysate from (5–15) × 10^9 cells was incubated with bait proteins bound to GST-Sepharose or anti-FLAG M2 affinity agarose (Sigma-Aldrich) for 1 h at 4°C. In coimmunoprecipitation experiments, WCL from wild-type cells or cells expressing FLAG-tagged Irc6p from the genomic locus were incubated with FLAG-affinity beads for 1 h at 4°C. Samples were washed in buffer Y and analyzed as in Fernandez and Payne (2006). For direct interaction tests between Ypt31p and Irc6p, purified GST or GST-Ypt31p bound to glutathione beads (10 µg) were incubated with 1 mM GDP or 1 mM GMPPNP for 30 min at room temperature. After separate preloading, FLAG-Irc6p or FLAG-Irc6p-K22A (20 µg) was added to the GST/GST-Ypt31p samples as indicated in Figure 5C. Protein-binding reactions were placed on a rotator and incubated for 30 min at 4°C. Samples were washed and analyzed using SDS–PAGE and Coomassie Blue staining.

Limited proteolysis

Irc6p was treated with chymotrypsin in 20 µl reactions containing 2.5 µg of purified Irc6p and 40 ng of protease in digest buffer (100 mM Tris-HCl, pH8, 10 mM $CaCl_2$) at 24°C. Proteolysis was stopped at different time points by adding 5 mM PMSF, and proteins were analyzed by SDS–PAGE and staining with Coomassie Blue.

ACKNOWLEDGMENTS

We thank Nava Segev, Peter Novick, and Manfred Schmitt for plasmids, strains, and antibodies; James Wohlschlegel and Ajay Vashisht for mass spectrometry; Michael Kim for technical assistance; and Michael Sawaya and Arthur Laganowsky for helpful discussions. We also thank the UCLA–U.S. Department of Energy (U.S. DOE) X-ray Crystallography Core Facility (supported by DOE grant DE-FC02-02ER63421) and the assistance team at Advanced Photon Source (APS) beamline ID24-C. Use of the APS is supported by the U.S. DOE under contract number DE-AC02-06CH11357. This work was supported by a Leopoldina Fellowship (BMBF LPD 9901/8-167) to S.G. and a National Institutes of Health grant (GM39040) to G.S.P.

REFERENCES

Alvaro D, Lisby M, Rothstein R (2007). Genome-wide analysis of Rad52 foci reveals diverse mechanisms impacting recombination. PLoS Genet 3, e228.

Benli M, Doring F, Robinson DG, Yang X, Gallwitz D (1996). Two GTPase isoforms, Ypt31p and Ypt32p, are essential for Golgi function in yeast. EMBO J 15, 6460–6475.

Bensen ES, Costaguta G, Payne GS (2000). Synthetic genetic interactions with temperature-sensitive clathrin in *Saccharomyces cerevisiae*. Roles for synaptojanin-like Inp53p and dynamin-related Vps1p in clathrin-dependent protein sorting at the *trans*-Golgi network. Genetics 154, 83–97.

Bensen ES, Yeung BG, Payne GS (2001). Ric1p and the ypt6p GTPase function in a common pathway required for localization of *trans*-Golgi network membrane proteins. Mol Biol Cell 12, 13–26.

Borlido J, Zecchini V, Mills IG (2009). Nuclear trafficking and functions of endocytic proteins implicated in oncogenesis. Traffic 10, 1209–1220.

Bourne HR, Sanders DA, McCormick F (1991). The GTPase superfamily: conserved structure and molecular mechanism. Nature 349, 117–127.

Carroll SY, Stirling PC, Stimpson HE, Giesselmann E, Schmitt MJ, Drubin DG (2009). A yeast killer toxin screen provides insights into a/b toxin entry, trafficking, and killing mechanisms. Dev Cell 17, 552–560.

Chen SH, Chen S, Tokarev AA, Liu F, Jedd G, Segev N (2005). Ypt31/32 GTPases and their novel F-box effector protein Rcy1 regulate protein recycling. Mol Biol Cell 16, 178–192.

Chen SH, Shah AH, Segev N (2011). Ypt31/32 GTPases and their F-Box effector Rcy1 regulate ubiquitination of recycling proteins. Cell Logist 1, 21–31.

Click ES, Stearns T, Botstein D (2002). Systematic structure-function analysis of the small GTPase Arf1 in yeast. Mol Biol Cell 13, 1652–1664.

Colovos C, Yeates TO (1993). Verification of protein structures: patterns of nonbonded atomic interactions. Protein Sci 2, 1511–1519.

Copic A, Starr TL, Schekman R (2007). Ent3p and Ent5p exhibit cargo-specific functions in trafficking proteins between the *trans*-Golgi network and the endosomes in yeast. Mol Biol Cell 18, 1803–1815.

Costaguta G, Stefan CJ, Bensen ES, Emr SD, Payne GS (2001). Yeast Gga coat proteins function with clathrin in Golgi to endosome transport. Mol Biol Cell 12, 1885–1896.

Donaldson JG, Jackson CL (2011). ARF family G proteins and their regulators: roles in membrane transport, development and disease. Nat Rev Mol Cell Biol 12, 362–375.

Duncan MC, Ho DG, Huang J, Jung ME, Payne GS (2007). Composite synthetic lethal identification of novel membrane traffic inhibitors. Proc Natl Acad Sci USA 104, 6235–6240.

Edeling MA, Smith C, Owen D (2006). Life of a clathrin coat: insights from clathrin and AP structures. Nat Rev Mol Cell Biol 7, 32–44.

Emsley P, Cowtan K (2004). Coot: model-building tools for molecular graphics. Acta Crystallogr D Biol Crystallogr 60, 2126–2132.

Fernandez GE, Payne GS (2006). Laa1p, a conserved AP-1 accessory protein important for AP-1 localization in yeast. Mol Biol Cell 17, 3304–3317.

Furuta N, Fujimura-Kamada K, Saito K, Yamamoto T, Tanaka K (2007). Endocytic recycling in yeast is regulated by putative phospholipid translocases and the Ypt31p/32p-Rcy1p pathway. Mol Biol Cell 18, 295–312.

Holm L, Rosenstrom P (2010). Dali server: conservation mapping in 3D. Nucleic Acids Res 38, W545–W549.

Hutagalung AH, Novick PJ (2011). Role of Rab GTPases in membrane traffic and cell physiology. Physiol Rev 91, 119–149.

Ito T, Chiba T, Ozawa R, Yoshida M, Hattori M, Sakaki Y (2001). A comprehensive two-hybrid analysis to explore the yeast protein interactome. Proc Natl Acad Sci USA 98, 4569–4574.

Jedd G, Mulholland J, Segev N (1997). Two new Ypt GTPases are required for exit from the yeast *trans*-Golgi compartment. J Cell Biol 137, 563–580.

Kelley LA, Sternberg MJ (2009). Protein structure prediction on the Web: a case study using the Phyre server. Nat Protoc 4, 363–371.

Kiefer F, Arnold K, Kunzli M, Bordoli L, Schwede T (2009). The SWISS-MODEL Repository and associated resources. Nucleic Acids Res 37, D387–D392.

Kirchhausen T (2000). Three ways to make a vesicle. Nat Rev Mol Cell Biol 1, 187–198.

Lambert C, Leonard N, De Bolle X, Depiereux E (2002). ESyPred3D: prediction of proteins 3D structures. Bioinformatics 18, 1250–1256.

Langer G, Cohen SX, Lamzin VS, Perrakis A (2008). Automated macromolecular model building for X-ray crystallography using ARP/wARP version 7. Nat Protoc 3, 1171–1179.

Li A, Liu Z, Li Q, Yu L, Wang D, Deng X (2008). Construction and characterization of bidirectional expression vectors in *Saccharomyces cerevisiae*. FEMS Yeast Res 8, 6–9.

Longtine MS, McKenzie A, Demarini DJ, Shah NG, Wach A, Brachat A, Philippsen P, Pringle JR (1998). Additional modules for versatile and economical PCR-based gene deletion and modification in *Saccharomyces cerevisiae*. Yeast 14, 953–961.

Luo R, Akpan IO, Hayashi R, Sramko M, Barr V, Shiba Y, Randazzo PA (2012). GTP-binding protein–like domain of AGAP1 is protein binding site that allosterically regulates ArfGAP protein catalytic activity. J Biol Chem 287, 17176–17185.

Marchler-Bauer A *et al*. (2011). CDD: a Conserved Domain Database for the functional annotation of proteins. Nucleic Acids Res 39, D225–D229.

McMahon HT, Boucrot E (2011). Molecular mechanism and physiological functions of clathrin-mediated endocytosis. Nat Rev Mol Cell Biol 12, 517–533.

Novick P, Field C, Schekman R (1980). Identification of 23 complementation groups required for post-translational events in the yeast secretory pathway. Cell 21, 205–215.

Ortiz D, Medkova M, Walch-Solimena C, Novick P (2002). Ypt32 recruits the Sec4p guanine nucleotide exchange factor, Sec2p, to secretory vesicles; evidence for a Rab cascade in yeast. J Cell Biol 157, 1005–1015.

Otwinowski Z, Minor W (1997). Processing of X-ray diffraction data collected in oscillation mode. Methods Enzymol 276, 307–326.

Page LJ, Sowerby PJ, Lui WW, Robinson MS (1999). γ-synergin: an EH domain-containing protein that interacts with γ-adaptin. J Cell Biol 146, 993–1004.

Panic B, Perisic O, Veprintsev DB, Williams RL, Munro S (2003). Structural basis for Arl1-dependent targeting of homodimeric GRIP domains to the Golgi apparatus. Mol Cell 12, 863–874.

Pape T, Schneider TR (2004). HKL2MAP: a graphical user interface for macromolecular phasing with SHELX programs. J Appl Crystallogr 37, 843–844.

Payne GS, Schekman R (1989). Clathrin—a role in the intracellular retention of a Golgi membrane protein. Science 245, 1358–1365.

Phan HL, Finlay JA, Chu DS, Tan PK, Kirchhausen T, Payne GS (1994). The Saccharomyces cerevisiae APS1 gene encodes a homolog of the small subunit of the mammalian clathrin AP-1 complex: evidence for functional interaction with clathrin at the Golgi complex. EMBO J 13, 1706–1717.

Rad MR, Phan HL, Kirchrath L, Tan PK, Kirchhausen T, Hollenberg CP, Payne GS (1995). *Saccharomyces cerevisiae* Apl2p, a homologue of the mammalian clathrin AP β subunit, plays a role in clathrin-dependent Golgi functions. J Cell Sci 108, 1605–1615.

Randazzo PA, Weiss O, Kahn RA (1995). Preparation of recombinant ADP-ribosylation factor. Methods Enzymol 257, 128–135.

Rao ST, Rossmann MG (1973). Comparison of super-secondary structures in proteins. J Mol Biol 76, 241–256.

Robinson MS (2004). Adaptable adaptors for coated vesicles. Trends Cell Biol 14, 167–174.

Sciorra VA, Audhya A, Parsons AB, Segev N, Boone C, Emr SD (2005). Synthetic genetic array analysis of the PtdIns 4-kinase Pik1p identifies components in a Golgi-specific Ypt31/rab-GTPase signaling pathway. Mol Biol Cell 16, 776–793.

Seeger M, Payne GS (1992). Selective and immediate effects of clathrin heavy chain mutations on Golgi membrane protein retention in *Saccharomyces cerevisiae*. J Cell Biol 118, 531–540.

Segev N (2011). Coordination of intracellular transport steps by GTPases. Semin Cell Dev Biol 22, 33–38.

Sheldrick GM (2010). Experimental phasing with SHELXC/D/E: combining chain tracing with density modification. Acta Crystallogr D Biol Crystallogr 66, 479–485.

Sikorski RS, Hieter P (1989). A system of shuttle vectors and yeast host strains designed for efficient manipulation of DNA in *Saccharomyces cerevisiae*. Genetics 122, 19–27.

Stenmark H (2009). Rab GTPases as coordinators of vesicle traffic. Nat Rev Mol Cell Biol 10, 513–525.

Traub LM (2005). Common principles in clathrin-mediated sorting at the Golgi and the plasma membrane. Biochim Biophys Acta 1744, 415–437.

Vagin AA, Steiner RS, Lebedev AA, Potterton L, McNicholas S, Long F, Murshudov GN (2004). REFMAC5 dictionary: organisation of prior chemical knowledge and guidelines for its use. Acta Crystallogr D Biol Crystallogr 60, 2284–2295.

Valdivia RH, Baggott D, Chuang JS, Schekman RW (2002). The yeast clathrin adaptor protein complex 1 is required for the efficient retention of a subset of late Golgi membrane proteins. Dev Cell 2, 283–294.

Wagner P, Molenaar CM, Rauh AJ, Brokel R, Schmitt HD, Gallwitz D (1987). Biochemical properties of the ras-related YPT protein in yeast: a mutational analysis. EMBO J 6, 2373–2379.

Wittinghofer A, Vetter IR (2011). Structure-function relationships of the G domain, a canonical switch motif. Annu Rev Biochem 80, 943–971.

Yeung BG, Phan HL, Payne GS (1999). Adaptor complex-independent clathrin function in yeast. Mol Biol Cell 10, 3643–3659.

Yu H *et al*. (2008). High-quality binary protein interaction map of the yeast interactome network. Science 322, 104–110.

Zhang W, Durocher D (2010). De novo telomere formation is suppressed by the Mec1-dependent inhibition of Cdc13 accumulation at DNA breaks. Genes Dev 24, 502–515.